https://doi.org/10.20965/jdr.2013.p0912

Paper:

Finite-Difference Simulation of Long-Period Ground Motion for the Nankai Trough Megathrust Earthquakes

Takahiro Maeda, Nobuyuki Morikawa, Asako Iwaki, Shin Aoi, and Hiroyuki Fujiwara

National Research Institute for Earth Science and Disaster Prevention
3-1 Tennodai, Tsukuba, Ibaraki 305-0006, Japan
E-mail: tmaeda@bosai.go.jp

[Received May 1, 2013; accepted September 2, 2013]

We evaluated long-period ground motions for the anticipated Nankai Trough megathrust earthquake in southwest Japan. To understand a variation of long-period ground motions caused by the uncertainty of the source model, we performed a finite difference simulation using 104 source models, assuming various possible source parameters, including rupture area, asperity configuration, and hypocenter location. For the variety of rupture areas, we included scenarios that have extremely huge rupture areas, as was proposed by the Japan Central Disaster Management Council of Cabinet Office after the 2011 Tohoku-Oki earthquake. We also included scenarios that have large slip areas near the trough following the lessons learned from the 2011 event. Simulated waveforms and response spectra show a large variation at a site. However, by grouping the simulation results with respect to the source area, we determined that scenarios with wider rupture areas have a larger peak ground velocity and velocity response than those with smaller rupture areas. The influence of the large slip near the trough causes later phases to be large and long. However, the later phases are decreased by using a boxcar-like slip velocity time function instead of a Kostrov-like function and by decreasing rupture velocity. The spatial distribution of the simulated peak ground velocity and velocity response show that the long-period ground motions are amplified particularly on sedimentary basins, where big cities have been established. It is important to consider how to account for the large variation of the simulation results in the seismic hazard assessment.

Keywords: Nankai Trough, long-period ground motion, megathrust earthquake, finite difference method

1. Introduction

Megathrust earthquakes in the Nankai Trough in southwest Japan have been occurring with an interval of 100–200 years (e.g., [1]). Mainly, there are two patterns of Nankai Trough earthquakes; one is a series of smaller earthquakes in a short time period (less than a few years) and the second is a single larger event rupturing at once. The most recent example of the first case is the series of earthquakes of the 1944 Tonankai earthquake (M7.9 [2]) and the 1946 Nankai earthquake (M8.0 [2]). The most recent example of the second case is the 1707 Hoei earthquake (M8.6 [2]). Although the Hoei earthquake has been regarded as the largest earthquake in the Nankai Trough, the Central Disaster Management Council (CDMC) of the Cabinet Office, Japan, proposed a hypothetical largest source area for a megathrust earthquake in the Nankai Trough following the lessons learned from the 2011 Tohoku-Oki earthquake (**Fig. 1b**). The Earthquake Research Committee (ERC) of the Headquarters for Earthquake Research Promotion, Japan, revised the long-term evaluation of earthquakes in the Nankai Trough by taking into account the hypothetical largest earthquake [2].

The megathrust earthquake potentially causes serious damage by long-period ground motion as well as strong ground motion and tsunamis. Damage of high-rise and large-scale structures due to the long-period ground motion has been observed during past large earthquakes (e.g., the 1964 Niigata earthquake, the 2003 Tokachi-Oki earthquake in Japan, and the 1985 Michoacan earthquake in Mexico). During the 2011 Tohoku-Oki earthquake in Japan, a high-rise building in Osaka city, about 800 km away from the epicenter, was damaged. This evidence suggests that the long-period ground motions potentially cause damage to structures even at long-distance basins. Along the Nankai Trough, big cities have been established on large basins: Tokyo on the Kanto basin, Nagoya on the Nobi basin, and Osaka on the Osaka basin (**Fig. 1**). Fortunately, high-rise and large-scale structures in these cities have not experienced megathrust earthquakes in the Nankai Trough. It is therefore important to evaluate long-period ground motions in order to improve seismic hazard assessment.

Long-period ground motion evaluation had been intended for past disastrous earthquakes prior to the 2011 event. For example, the ERC published long-period ground motion hazard maps in 2009 [3] and 2012 [4]. These maps evaluated three Nankai Trough earthquakes; two past earthquakes – the 1944 Tonankai and 1946 Nankai earthquakes – and a hypothetical Tokai earthquake. As mentioned above, the Nankai Trough earthquake has various occurrence patterns, so ground motion evaluation based on a few specific earthquakes is insuffi-

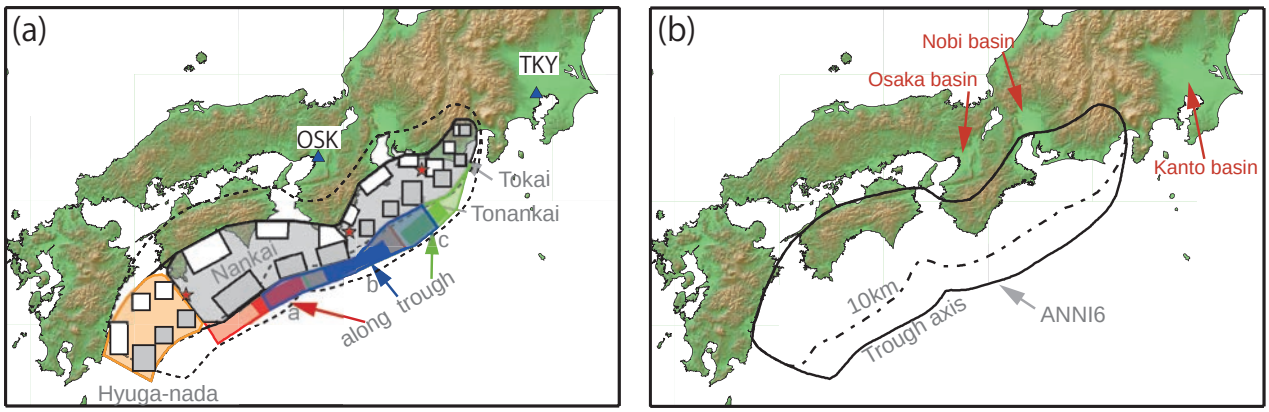

Fig. 1. Source models for the Nankai Trough earthquakes. (a) Grey regions are the source areas of the Nankai, Tonankai, and hypothetical Tokai earthquakes. The orange region is a source area of Hyuga-nada. Red, blue, and green regions are source areas along the trough. Solid and open squares in the source area are asperities of shallower and deeper cases, respectively. Red stars are the hypocenters. Blue triangles are the sites for comparing simulation results. (b) Source area for the hypothetical largest earthquake.

cient.

This study aims to present a possible range of long-period ground motions generated by the anticipated megathrust earthquake in the Nankai Trough by taking into account the uncertainty of the source model. Thus, we evaluate long-period ground motions using many scenarios with various possible parameters including the rupture area, asperity configuration, and hypocenter location. We also include scenarios that have extremely huge source area, as proposed by the CDMC. The long-period ground motions are simulated by the finite difference method using a "characterized source model," which will be explained in the next section, and a recently developed three-dimensional underground structure model of Japan.

2. Seismic Source Model

The source models are constructed by following the ground motion evaluation of the Nankai Trough earthquake published by the ERC [3, 5]. The characterized source model is used in the long-period ground motion simulation. The characterized source model is defined by three kinds of parameters: outer, inner, and extra fault parameters. These parameters are determined based on a "recipe" for predicting strong ground motion [6, 7]. Although the recipe for the crustal earthquake has been verified using observed records of many earthquakes, the recipe for the subduction-zone earthquake has been validated using insufficient data, particularly for megathrust earthquakes. We should note that the ground-motion simulation results will be modified after improving the recipe for the subduction-zone earthquake.

We consider a variety of source parameters. For conventional models (except for the hypothetical largest source model), the rupture area, asperity configuration, hypocenter location, and slip velocity function are the variables. In addition to these variables, the distribution of the seismic moment and rupture velocity are the variables for the hypothetical largest source model. We do not assume random heterogeneity of slip, rupture velocity, and other parameters. We should note that the present results are still within limited assumptions.

2.1. Outer Fault Parameter

First, we determined the outer fault parameters that define an overall character of the source model. We defined source areas of the anticipated Nankai Trough earthquakes as shown in **Fig. 1**. An occurrence pattern of the Nankai Trough earthquakes is assumed: the respective earthquakes occur independently or multiple earthquakes occur in a correlated manner. For the respective earthquakes, we defined source areas of the Nankai earthquake (ANNKI), the Tonankai earthquake (ATNKI), and the hypothetical Tokai earthquake (ATOKI) based on the model proposed by [8]. The Hyuga-nada area (AHGND) was also modeled as a source area, since [9] noted that a source area of the 1707 Hoei earthquake extends to this area. We also assumed a large slip area along the trough following the lessons learned from the 2011 Tohoku-oki earthquake and modeled three source areas along the trough (**Fig. 1a**; ATRGHa-c).

We modeled source areas for the case of correlated occurrence as a combination of the respective source areas (**Fig. 2**). These are the Nankai-Tonankai area (ANNI1), the Tonankai-hypothetical Tokai area (ANNI2), the Nankai-Tonankai-hypothetical Tokai area (ANNI3), the Nankai -Tonankai-hypothetical Tokai area with the along trough area (ANNI4a-c), and the Nankai-Tonankai-hypothetical Tokai area with the Hyuga-nada area (ANNI5). Before the 2011 Tohoku-Oki earthquake, ANNI3 or ANNI5 were regarded as the largest source areas for the Nankai Trough earthquake.

In addition to the above conventional source models, we modeled the source area corresponding to the hypothetical largest earthquake in the Nankai Trough proposed by the CDMC (ANNI6; **Fig. 1b**). This source area is expanded especially in the along-dip direction of the Philippine-Sea plate, compared to the conventional source

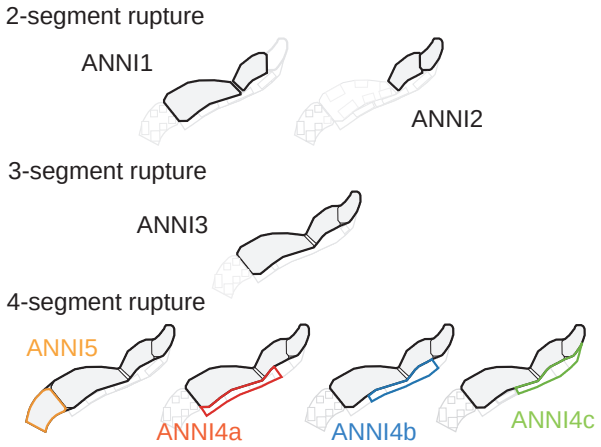

Fig. 2. Source areas for the case of correlated occurrence of respective earthquakes.

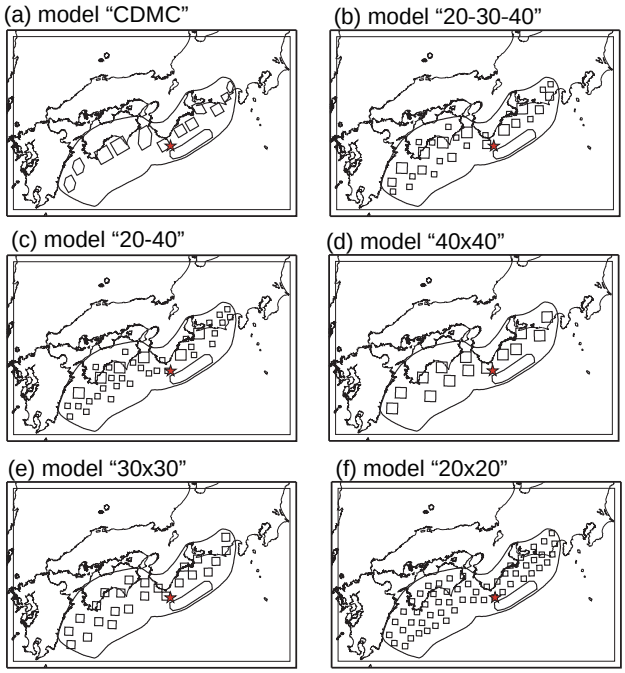

Fig. 3. Asperity configuration for the ANNI6 source models.

areas. The depth range of the source area is from the trough axis to the down-dip limit of the deep long-period tremors (around 40 km depth). Although the CDMC assumes that the source area at depths shallower than 10 km does not contribute to strong ground motion generation, we included this area for the calculation of long-period ground motion.

The rupture area S for each source area is estimated by taking into account the geometry of the plate interface and then calculating the seismic moment M_0 using the circular crack model [10], assuming an average stress drop $\Delta\sigma_c$ of 3.0 MPa [11, 12] and an average slip D by assuming the rigidity of 40.4 GPa.

We treated the source area of ANNI6 in two manners based on the recipe: one assumes a single segment and the other assumes two segments (cases "m1" and "m2" in **Table 2**). For the case m2, the two segments are the source areas for the areas deeper and shallower than 10 km, respectively, and distribute the seismic moment between the two segments so that the average stress drop will be the same for each segment. In the following, we use the terms "deep segment" and "shallow segment" not only for the case m2 but also for the case m1 for the sake of convenience. Although the total seismic moments for cases m1 and m2 are the same, the case m1 has larger seismic moment on the shallow segment than dose case m2 (**Table 2**). Thus, the contributions of the deep and shallow segments can be distinguished by comparing the results for cases m1 and m2.

2.2. Inner Fault Parameter

Next, we determined the inner fault parameters that define the property of asperities. The combined area of asperities (large slip areas) S_a and the average slip of asperities D_a are derived by a scaling relationship proposed by [13]: $S_a = 0.2S$ and $D_a = 2.2D$. We adopted the above scaling relationship and average stress drop of 3.0 MPa by following the strong-motion evaluation of the hypothetical Tokai earthquake [3]. Although the original result of [13] has an average stress drop of 1.4 MPa, we considered that 3.0 MPa is an acceptable value consistent with [13] by considering a standard deviation of the relationship.

For the conventional model, the number of asperity for the ANNKI, ATNKI, ATOKI, and AHGND source areas is three and their area ratio is 2 : 1 : 1 [5], while the number of asperity for ATRGHa-c areas is one. Two patterns of asperity configuration are assumed for ANNKI, ATNKI, ATOKI, and AHGND areas: deeper and shallower cases (**Fig. 1a**). Because the generation of surface waves, which affect long-period ground motion, depends strongly on source depth, the assumed asperity patterns may cover a broad range of excitation efficiency of the surface wave. For the case of a correlated occurrence, we assume that the size and location of asperity is same as the respective earthquake and calculate the average slip and seismic moment with respect to a total rupture area. Source parameters for the conventional models are shown in **Table 1**.

The source area of ANNI6 is large and not expressed as a combination of respective earthquakes from the conventional model. Thus, we arrange the asperities in a manner different from that we did for the conventional model. Six patterns of asperity configuration are assumed for the deep segment (**Fig. 3**). The model "CDMC" has a similar asperity configuration to the source model for calculating the strong motion proposed by the CDMC: the shape and location are similar but the sizes are enlarged so that the combined asperity area will be 20% of the total area. Other models consist of fixed-size asperities. We put the largest asperities (40 km × 40 km) of model – "20-30-40," "20-40," and "40×40" – on similar positions as those of the model "CDMC." Smaller asperities (20 km × 20 km and 30 km × 30 km) are introduced to avoid a lack of short period contents, because heterogeneity within the

Table 1. Source parameters for the conventional models.

				ANNKI	ATNKI	ATOKI	ATRGH	AHGND	ANNI1	ANNI2	ANNI3	ANNI4	ANNI5
Total			S (km^2)	35800	14500	9400	12500	19000	51200	23600	60300	72800	80500
			M_0 (Nm)	8.3×10^{21}	2.2×10^{21}	1.1×10^{21}	1.7×10^{21}	3.2×10^{21}	1.4×10^{22}	4.5×10^{21}	1.8×10^{22}	2.4×10^{22}	2.8×10^{22}
			Mw	8.5	8.2	8.0	8.1	8.3	8.7	8.4	8.8	8.9	8.9
			$\Delta\sigma$ (MPa)	3.0									
			density(kg/m^3)	2800									
			Vs (m/s)	3800									
			rigidity (GPa)	40.4									
			Vr (m/s)	2700									
			f_{max}(Hz) [7]	13.5									
asperity	Nankai	1	S (km^2)	3580	-	-	-	-	3580	-	3580	3580	3580
			M_{0a} (Nm)	2.1×10^{21}	-	-	-	-	2.9×10^{21}	-	3.3×10^{21}	3.6×10^{21}	4.0×10^{21}
			$\Delta\sigma_a$ (MPa)	15.0	-	-	-	-	15.3	-	15.2	15.1	15.3
		2,3	S (km^2)	1790	-	-	-	-	1790	-	1790	1790	1790
			M_{0a} (Nm)	7.6×10^{20}	-	-	-	-	1.0×10^{21}	-	1.2×10^{21}	1.3×10^{21}	1.4×10^{21}
			$\Delta\sigma_a$ (MPa)	15.0	-	-	-	-	15.3	-	15.2	15.1	15.3
	Tonankai	1	S (km^2)	-	1450	-	-	-	1450	1450	1450	1450	1450
			M_{0a} (Nm)	-	5.5×10^{20}	-	-	-	7.4×10^{20}	7.7×10^{20}	8.6×10^{20}	9.2×10^{20}	1.0×10^{21}
			$\Delta\sigma_a$ (MPa)	-	15.0	-	-	-	15.3	14.8	15.2	15.1	15.3
		2,3	S (km^2)	-	725	-	-	-	725	725	725	725	725
			M_{0a} (Nm)	-	2.0×10^{20}	-	-	-	2.6×10^{20}	2.7×10^{20}	3.0×10^{20}	3.2×10^{20}	3.6×10^{20}
			$\Delta\sigma_a$ (MPa)	-	15.0	-	-	-	15.3	14.8	15.2	15.1	15.3
	Tokai	1	S (km^2)	-	-	940	-	-	-	940	940	940	940
			M_{0a} (Nm)	-	-	2.9×10^{20}	-	-	-	4.0×10^{20}	4.5×10^{20}	4.8×10^{20}	5.4×10^{20}
			$\Delta\sigma_a$ (MPa)	-	-	15.0	-	-	-	14.8	15.2	15.1	15.3
		2,3	S (km^2)	-	-	470	-	-	-	470	470	470	470
			M_{0a} (Nm)	-	-	1.0×10^{20}	-	-	-	1.4×10^{20}	1.6×10^{20}	1.7×10^{20}	1.9×10^{20}
			$\Delta\sigma_a$ (MPa)	-	-	15.0	-	-	-	14.8	15.2	15.1	15.3
	along trough	a,b,c	S (km^2)	-	-	-	2500	-	-	-	-	2500	-
			M_{0a} (Nm)	-	-	-	7.6×10^{20}	-	-	-	-	2.1×10^{21}	-
			$\Delta\sigma_a$ (MPa)	-	-	-	15.0	-	-	-	-	15.1	-
	Hyuganada	1	S (km^2)	-	-	-	-	1900	-	-	-	-	1900
			M_{0a} (Nm)	-	-	-	-	8.3×10^{20}	-	-	-	-	1.5×10^{21}
			$\Delta\sigma_a$ (MPa)	-	-	-	-	15.0	-	-	-	-	15.3
		2,3	S (km^2)	-	-	-	-	950	-	-	-	-	950
			M_{0a} (Nm)	-	-	-	-	2.9×10^{20}	-	-	-	-	5.4×10^{20}
			$\Delta\sigma_a$ (MPa)	-	-	-	-	15.0	-	-	-	-	15.3
Back ground			S (km^2)	28640	11600	7520	10000	15200	41140	18820	48360	58360	64760
			M_{0b} (Nm)	4.7×10^{21}	1.2×10^{21}	6.3×10^{20}	9.6×10^{20}	1.8×10^{21}	8.1×10^{21}	2.5×10^{21}	1.0×10^{22}	1.4×10^{22}	1.6×10^{22}
			$\Delta\sigma_b$ (MPa)	1.8	1.8	1.8	3.0	1.8	1.4	1.3	1.2	1.1	1.0

asperities is not assumed. A size distribution of models "20-30-40" and "20-40" is arbitrarily assumed and does not follow any kind of source model, such as the k^{-2} model [14]. The models "20×20" and "30×30" are experimental to see the effect of the asperity sizes. Asperity sizes of 20 km × 20 km, 30 km × 30 km, and 40 km × 40 km are approximately similarly sized to the asperities assumed in the conventional model (**Table 1**). For the shallow segment, we assumed a large slip area on eastern part of the segment. Source parameters for ANNI6 scenarios are shown in **Table 2**.

We used a Kostrov-like slip velocity time function proposed by [15]. This function was approximated from a dynamic rupture simulation. Applying this function to the interplate earthquake is a contentious issue, especially in a shallow source area. The shallowest region of subduction zone is considered to be a region where tsunami earthquakes that have a slow rupture velocity can occur and where events that have longer rupture durations than do deeper events with the same seismic moment can also occur [16]. Because the Kostrov-like function may not be most appropriate for this region, we also applied a boxcar-like time function (slip velocity of 1.0 m/s) to the shallow segment as diametrical opposites.

We assumed a rupture velocity V_r of 2.7 km/s, which is approximately 70% of the S-wave velocity

Table 2. Source parameters for the ANNI6 scenarios.

S (km^2)	144030 (= 110360 + 33670)
M_0 (Nm)	6.7×10^{22}
$\Delta\sigma$(MPa)	3.0
Mw	9.2
fmax (Hz) [7]	13.5

	p1	p2#	p3#
density (kg/m^3)	2800	2800	2650
Vs (m/s)	3800	3800	3200
rigidity (GPa)	40.4	40.4	27.1
Vr (m/s)	2700	2300	2300

applied only to the shallow segment

				m1			m2			
							p1, p2	p3		
		number of asperity	Area km^2	Slip m	M_0 Nm	$\Delta\sigma$ MPa	Slip m		M_0 Nm	$\Delta\sigma$ MPa
model 20×20										
deep	asperity	55	400	14.7	2.4×10^{20}	15.0	28.4		4.6×10^{20}	19.2
	back ground	-	88360	8.1	2.9×10^{22}	0.6	9.1		3.2×10^{22}	0.5
shallow	asperity	1	6734	60.4	1.6×10^{22}	15.0	15.7	23.4	4.3×10^{21}	19.1
	back ground	-	26936	8.1	8.8×10^{21}	0.6	5.0	7.4	5.4×10^{21}	3.9
model 30×30										
deep	asperity	24	900	18.0	6.6×10^{20}	15.2	28.4		1.0×10^{21}	19.6
	back ground	-	88760	8.2	2.9×10^{22}	0.8	9.1		3.3×10^{22}	0.8
shallow	asperity	1	6734	49.2	1.3×10^{22}	15.2	15.7	23.4	4.3×10^{21}	19.1
	back ground	-	26936	8.2	8.9×10^{21}	0.8	5.0	7.4	5.4×10^{21}	3.9
model 40×40										
deep	asperity	14	1600	20.5	1.3×10^{21}	14.8	28.4		1.8×10^{21}	18.9
	back ground	-	87960	8.0	2.9×10^{22}	0.9	9.0		3.2×10^{22}	1.0
shallow	asperity	1	6734	42.0	1.1×10^{22}	14.8	15.7	23.4	4.3×10^{21}	19.1
	back ground	-	26936	8.0	8.8×10^{21}	0.9	5.0	7.4	5.4×10^{21}	3.9
model 20-40										
deep	asperity	6	1600	24.7	1.6×10^{21}	15.0	39.5		2.6×10^{21}	19.2
	asperity	31	400	12.3	2.0×10^{20}	15.0	19.8		3.2×10^{20}	19.2
	back ground	-	88360	8.1	2.9×10^{22}	0.7	9.1		3.2×10^{22}	0.7
shallow	asperity	1	6734	50.6	1.4×10^{22}	15.0	15.7	23.4	4.3×10^{21}	19.1
	back ground	-	26936	8.1	8.8×10^{21}	0.7	5.0	7.4	5.4×10^{21}	3.9
model 20-30-40										
deep	asperity	6	1600	23.4	1.5×10^{21}	15.1	35.9		2.3×10^{21}	19.3
	asperity	7	900	17.5	6.4×10^{20}	15.1	26.9		9.8×10^{20}	19.3
	asperity	15	400	11.7	1.9×10^{20}	15.1	18.0		2.9×10^{20}	19.3
	back ground	-	88460	8.1	2.9×10^{22}	0.8	9.1		3.2×10^{22}	0.8
shallow	asperity	1	6734	48.0	1.3×10^{22}	15.1	15.7	23.4	4.3×10^{21}	19.1
	back ground	-	26936	8.1	8.8×10^{21}	0.8	5.0	7.4	5.4×10^{21}	3.9
model CDMC										
deep	asperity	2	1905	20.4	1.6×10^{21}	15.0	27.1		2.1×10^{21}	19.2
	asperity	2	2822	24.9	2.8×10^{21}	15.0	32.9		3.8×10^{21}	19.2
	asperity	1	3527	27.8	4.0×10^{21}	15.0	36.8		5.3×10^{21}	19.2
	asperity	1	1587	18.7	1.2×10^{21}	15.0	24.7		1.6×10^{21}	19.2
	asperity	4	1471	18.0	1.1×10^{21}	15.0	23.8		1.4×10^{21}	19.2
	asperity	2	789	13.2	4.2×10^{20}	15.0	17.4		5.6×10^{20}	19.2
	back ground	-	88330	8.1	2.9×10^{22}	1.0	9.0		3.2×10^{22}	102
shallow	asperity	1	6734	38.4	1.0×10^{22}	15.0	15.7	23.4	4.3×10^{21}	19.1
	back ground	-	26936	8.1	8.8×10^{21}	1.0	5.0	7.4	5.4×10^{21}	3.9

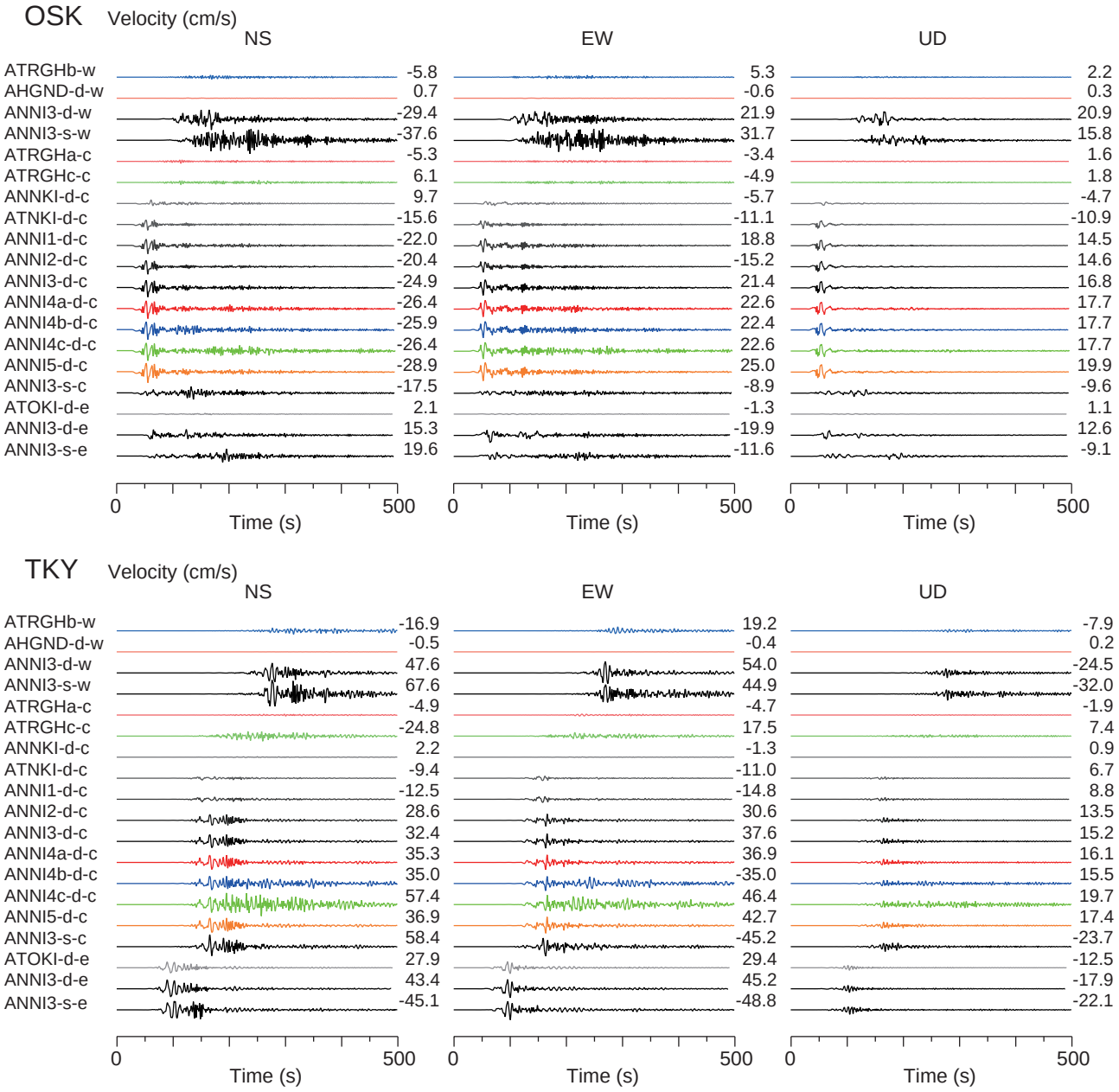

Fig. 4. Results of the 3-D FD simulation for 19 scenarios at OSK (upper) and TKY (lower). The scenario name shown in the left means [source area]-[asperity location (deep, shallow)]-[hypocenter (west, center, east)]. The numbers on the right indicate the peak amplitude in cm/s. The waveforms are band-pass filtered at 0.03-0.3 Hz.

(3.8 km/s) [17]. For the ANNI6 scenarios, we assumed a variation of rupture velocities for the shallow segment. Because a part of the shallow segment penetrates into a lower S-wave velocity (3.2 km/s) region in the velocity structure model used in the ground motion simulation, we included a case "p2" that has a smaller V_r (2.3 km/s). This means that we assumed larger S-wave velocity and density for the shallow segment in the case "p1." For the case p1, the rupture velocity of a part of the shallow segment is approximately 84% of the S-wave velocity. In addition, rigidity, which is derived from the S-wave velocity and density, is a parameter for the assumed slip velocity time function [15]; thus, we assumed a case "p3" having smaller values for V_r, S-wave velocity, and density (cases "p1," "p2," and "p3" in **Table 2**).

The slip angle is derived from a local orientation of the fault plane and a direction of fault motion, which is the angle of the relative motion of the hanging wall (continental plate) against the foot wall (Philippine-Sea plate). We assumed the direction of fault motion to be N125°E [8] uniformly over the fault.

2.3. Extra Fault Parameter

Finally, we determined the extra fault parameters that define a propagation pattern of rupture. We assumed three hypocenters: west (boundary of the Nankai and Hyuganada areas), center (boundary of Nankai and Tonankai areas), and east (boundary of the Tonankai and Tokai areas).

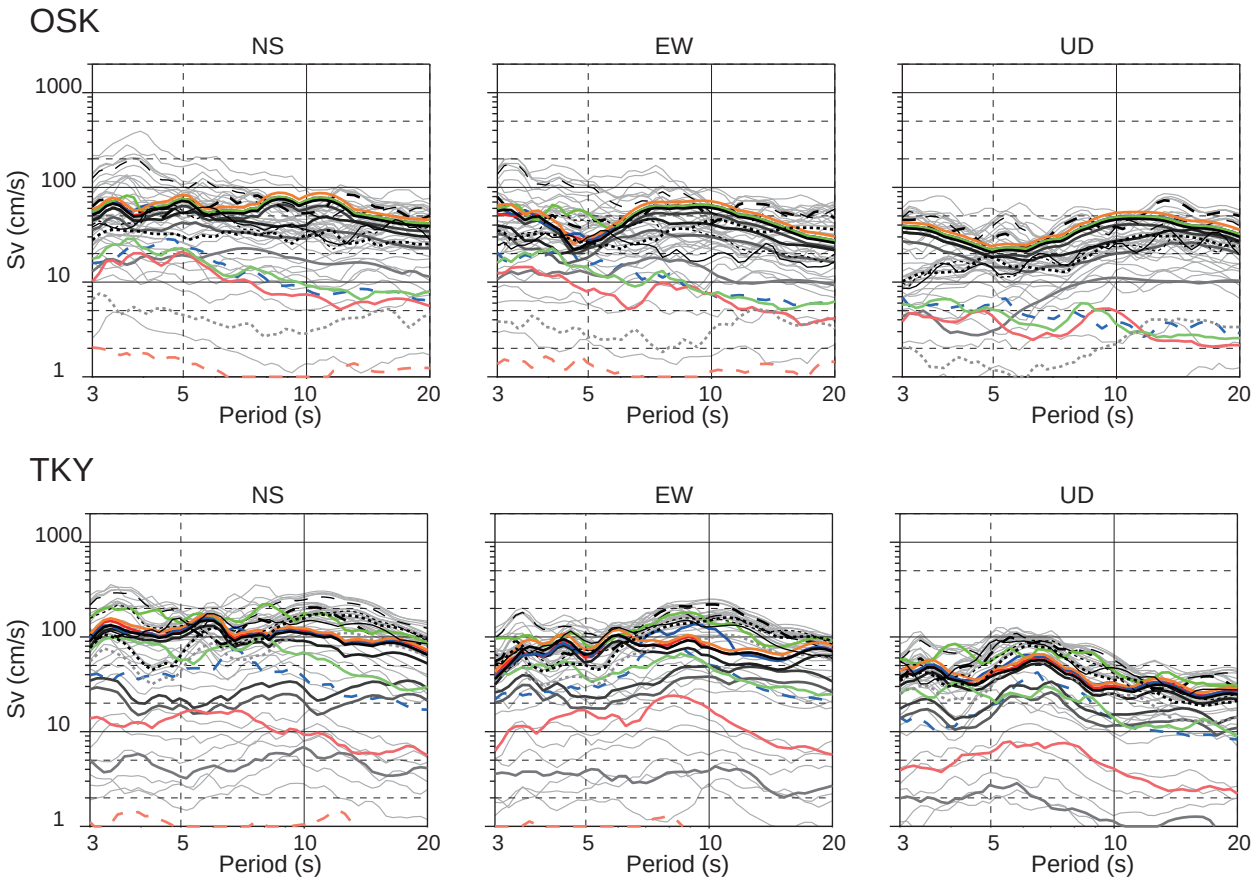

Fig. 5. Simulated velocity response spectra (damping factor $H = 0.05$) for the conventional model at OSK and TKY. Colored lines correspond to waveforms shown in **Fig. 4**. Dashed and dotted lines are west-hypocenter and east-hypocenter scenarios, respectively. Grey lines are the other scenarios.

The rupture propagates radially from the hypocenter at the assumed rupture velocity (**Table 2**). The rupture in each asperity starts from a point when the rupture front reaches the point.

3. Long-Period Ground Motion Simulations

The long-period ground motions are simulated using a three dimensional (3-D) finite difference (FD) method [18, 19]. To accommodate details of the 3-D subsurface structure into the FD model, we used discontinuous grids that consist of a fine grid spacing of 200 m in the horizontal and of 100 m in the vertical for regions shallower than 8 km that contain low-velocity sedimentary layers, and a three times coarser grid spacing for deeper region (8-70 km). The total number of grid points is about two billion. The 3-D velocity structure model used in the FD simulation is the Japan integrated velocity structure model [4, 20], which includes basin, crust, plate and oceanic structures. Although the original model has the lowest S-wave velocity of 350 m/s in the first layer, we fill the first layer with a second layer that has an S-wave velocity of 500 m/s in order to ensure the stability of the FD simulation. Considering the lowest S-wave velocity and grid spacing, our simulation is valid for periods longer than two seconds. However, because the characterized source model may not sufficiently support short period components, we should interpret the reliable period of the simulation with caution. We considered that the periods longer than five seconds rather than two seconds are valid for further analysis. Inelastic attenuation is introduced in the same way as in [21] and we assumed a reference period for Q-values of five seconds.

4. Results

We simulated long-period ground motions for 104 source models. **Figs. 4** and **5** compare the simulated ground velocities and velocity response spectra for the conventional model at Osaka (OSK) and Shinjuku in Tokyo (TKY). In **Fig. 4**, the ANNI3-d-c scenario (ANNI3 area with deeper asperity and central hypocenter) should be regarded as a reference: it does not be interpreted to mean that we consider this scenario to be the most plausible one. At OSK, direct waves predominate for the deep-asperity scenarios, while later phases predominate for the shallow-asperity scenarios. The contribution of the ATNKI area is dominant for center-hypocenter scenarios, while the contribution of the ANNKI area is dominant for the west-hypocenter scenarios. The velocity response

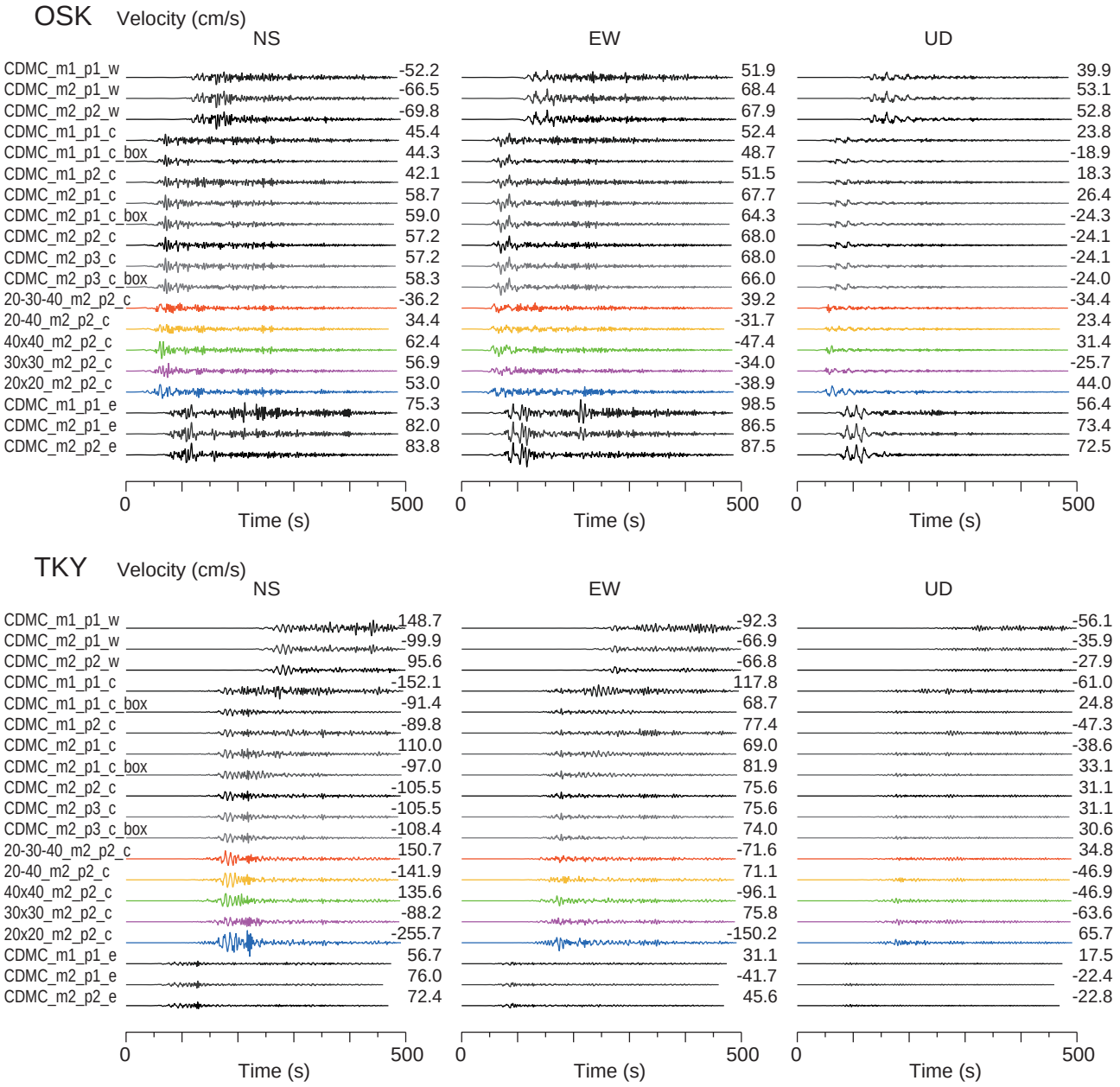

Fig. 6. Results of the 3-D FD simulation for ANNI6 scenarios at OSK (upper) and TKY (lower). The scenario name shown in the left means [asperity configuration (CDMC, 20-30-40, 20-40, 20×20, 30×30, 40×40)]- [seismic moment distribution (m1, m2)]- [extra fault parameter (p1, p2, p3)]- [hypocenter (west, center, east)]-[boxcar like source function]. The numbers on the right indicate the peak amplitude in cm/s. The waveforms are band-pass filtered at 0.03-0.3 Hz.

spectra for west-hypocenter scenarios exceed 100 cm/s for periods ranging between three and five seconds. At TKY, velocity waveforms for the west-hypocenter scenarios have slightly larger amplitudes than those for the other hypocenters. TKY is located on the eastward extension of the source area, so the rupture directivity effect is significant. The waveform difference between the two asperity configurations is smaller than those at OSK. This is because TKY is affected strongly by the ATOKI area, where two asperity configurations have small differences in depth. Later phases from the along trough "b" and "c" areas elongate the duration of long-period ground motion. The velocity response spectra exceed 100 cm/s for the broad period range. We could not recognize specific spectral peaks common to all simulated spectra at each site.

Figures 6 and **7** compare the simulated ground velocities and velocity response spectra for ANNI6 scenarios at OSK and TKY. In **Fig. 6**, the CDMC_m2_p2_c scenario is regarded as a reference. Waveforms and spectra have larger amplitudes than those in **Figs. 4** and **5**. The influence of the shallow segment appears in later phases in the east-hypocenter scenarios at OSK, and in the west- and center-hypocenter scenarios at TKY. The case m1 has larger later phases than does case m2 (e.g., CDMC_m1_p1_e at OSK and CDMC_m1_p1_c

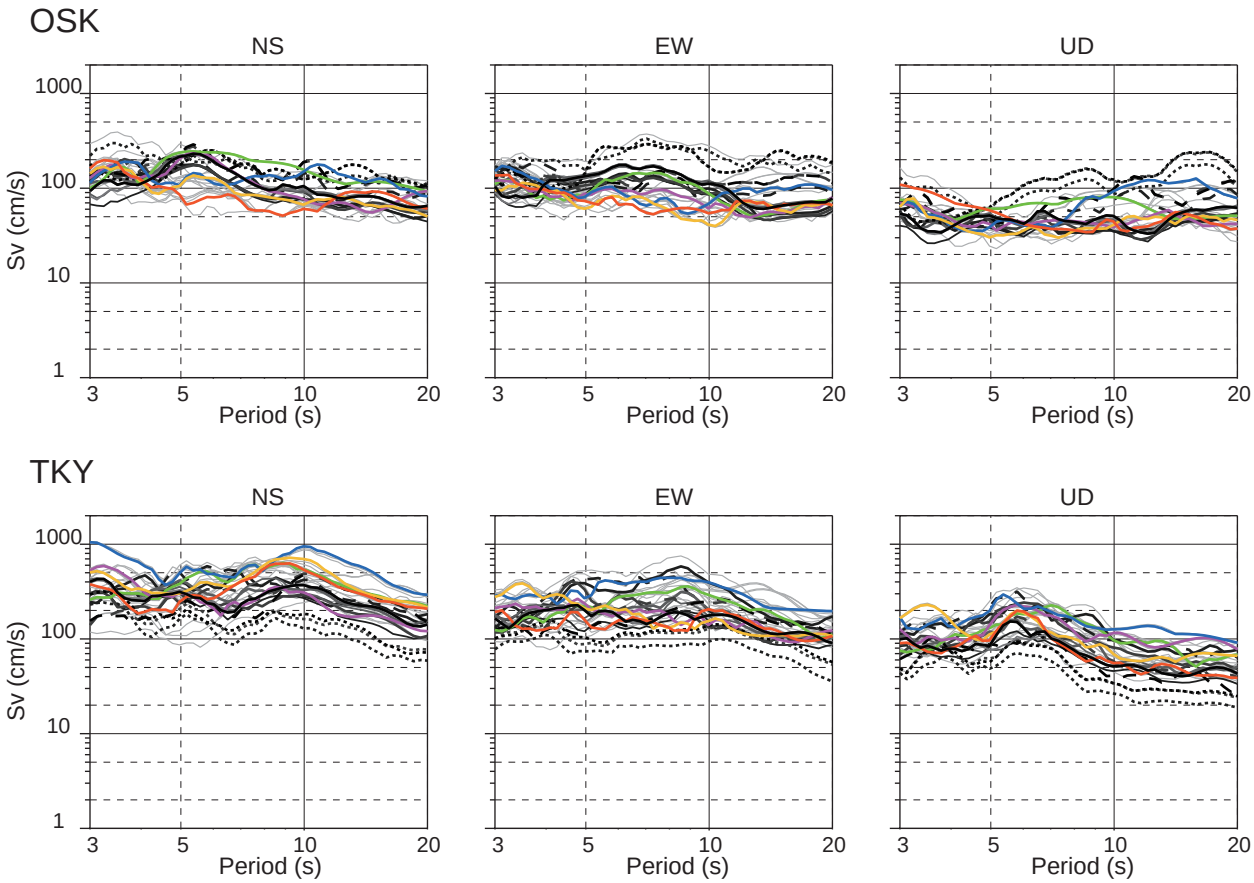

Fig. 7. Simulated velocity response spectra (damping factor $H = 0.05$) for ANNI6 scenarios at OSK and TKY. Colored lines correspond to waveforms shown in **Fig. 6**. Dashed and dotted lines are west-hypocenter and east-hypocenter scenarios, respectively. Grey lines are the other scenarios.

at TKY). However the later phases are decreased by using the boxcar-like slip velocity time function (case "m1_p1_box") and by decreasing the rupture velocity (case "m1_p2") on the shallow segment. This suggests that investigating the appropriate slip velocity function and rupture velocity, especially for the shallow segment, is important. Little difference in waveforms between cases p2 and p3 indicates that the S-wave velocity and density have insignificant effects on the assumed slip velocity function [15]. Waveforms and spectra vary with the asperity configuration, but systematic differences related to the asperity size are unclear. Simulated ground motions are affected by the asperity size and the asperity configuration. We consider that the influence of the asperity configuration makes it difficult to identify systematic differences in waveforms and spectra related to the asperity size.

5. Discussion and Conclusions

Figure 8 shows histograms of simulated peak ground velocity (PGV) and velocity response (S_v) at natural periods of 5, 7, and 10 s; we abbreviate those responses as S_v-5s, S_v-7s, and S_v-10s, respectively. We divide the simulated scenarios into five groups with respect to the occurrence pattern; (a) respective earthquakes (15 cases), (b) 2-segment earthquakes (10 cases), (c) 3-segment earthquake (6 cases), (d) 4-segment earthquakes (26 cases), and (e) hypothetical largest earthquake (47 cases). Note that groups "a" and "b" contain scenarios with quite different source areas. If we admit a general property that larger earthquakes have smaller occurrence probability, these groups can be related to an occurrence probability of the Nankai Trough earthquakes. These results should be regarded as a probability distribution, and it is important to investigate an appropriate distribution.

The scenarios with wider rupture areas (lower occurrence probability) have larger PGV and S_v values than those with smaller rupture areas (higher occurrence probability). In particular, ANNI6 scenarios have large averages and large variations of PGV and S_v values. We cannot simply compare the distribution of groups "a"-"d" with that of group "e," because the variety of source models for the ANNI6 scenarios is somewhat different from that for the other scenarios. However, these large variations suggest that the long-period ground motion evaluation based on a few specific scenarios is insufficient for the hazard assessment.

In **Fig. 8**, we also plot the results from previous studies on the long-period ground motion evaluation for the Nankai Trough earthquakes published by the ERC [3, 4].

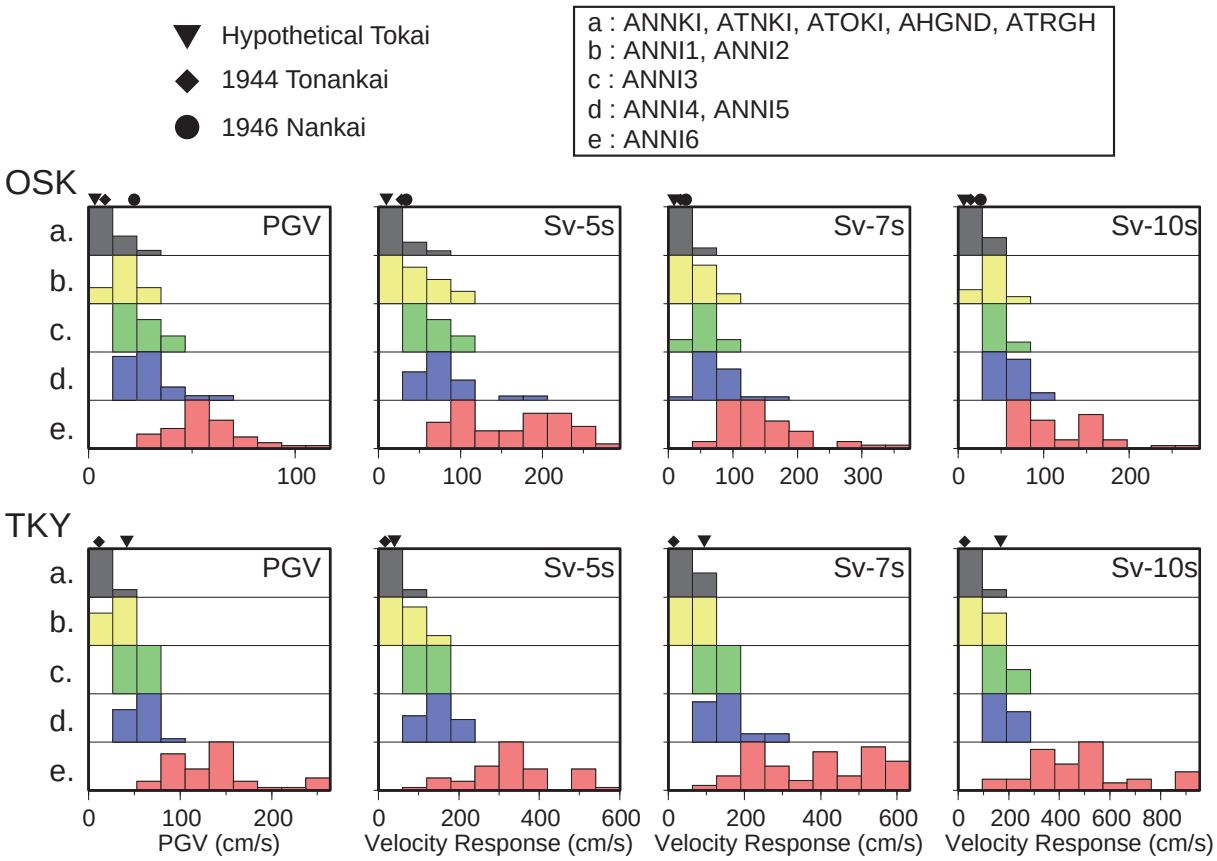

Fig. 8. Histograms of peak ground velocity (PGV) and velocity response (S_v) at periods of 5, 7, and 10 seconds for 104 scenarios at OSK and TKY. Histograms are color-coded according to the occurrence pattern. Symbols shown on top of each panel are the results from previous studies on the long-period ground motion evaluation for the Nankai Trough earthquakes published by the ERC [3, 4].

These PGV and S_v values for the 1944 Nankai, 1946 Tonankai, and Hypothetical Tokai earthquakes are consistent with those for group "a" of our study.

To assess the characteristics of the PGV and S_v distributions (**Fig. 8**), we make PGV and S_v (periods of 5 and 10 s) maps showing median (second quartile) and interquartile range (iqr: the difference between the third and first quartiles) using simulation results for five groups (**Figs. 9** and **10**). Large median values on the accretionary prism along the Nankai Trough suggest that this region greatly contributes to the generation and propagation of long-period ground motions. These maps clearly show that the long-period ground motions are amplified, particularly on sedimentary basins. Median values in these basins for group "e" are ∼2-3 times larger than those for group "c," which corresponds to the conventional largest scenario. In the median value maps, S_v-5s values are larger than S_v-10s values at the Osaka and Nobi basins, while the S_v-10s values are larger than the S_v-5s values at the Kanto basin, indicating a different response of the basins. These maps show a distribution of predicted long-period ground motions for the anticipated megathrust earthquake in the Nankai Trough with respect to the occurrence probability. It is important to recognize the uncertainty of the source model and then incorporate the large variation of the predicted results into the hazard assessment of long-period ground motions.

Acknowledgements

Some of the figures in this paper were made using GMT [22]. This manuscript was greatly improved by constructive comments by two anonymous reviewers. This study was supported by the Support Program for Long-Period Ground Motion Hazard Maps of Ministry of Education, Culture, Sport, Science, and Technology (MEXT).

References:

[1] K. Ishibashi, "Status of historical seismology in Japan," Ann. Geophys., Vol.47, pp. 339-368, 2004.

[2] Earthquake Research Committee, "On the long-term evaluation of earthquakes in the Nankai Trough (2nd edition)," 2013 (in Japanese), http://www.jishin.go.jp/main/chousa/13may_nankai/index.htm [accessed September 23, 2013]

[3] Earthquake Research Committee, "Long-period grond motion hazard maps for Japan," 2009 (in Japanese), http://www.jishin.go.jp/main/chousa/09_choshuki/index.htm [accessed September 23, 2013]

[4] Earthquake Research Committee, "Long-period grond motion hazard maps for Japan," 2012 (in Japanese), http://www.jishin.go.jp/main/chousa/12_choshuki/index.htm [accessed September 23, 2013]

[5] Earthquake Research Committee, "On the strong ground motion evaluation of earthquakes in the Nankai Trough," 2001 (in Japanese), http://www.jishin.go.jp/main/kyoshindo/01b/index.htm [accessed September 23, 2013]

[6] K. Irikura and H. Miyake, "Prediction of strong ground motions for scenario earthquakes," Journal of Geography, Vol.110, pp. 849-875, 2001 (in Japanese with English abstract).

[7] Earthquake Research Committee, "Strong Ground Motion Prediction Method ("Recipe") for Earthquakes with Specified Source Faults," 2009 (in Japanese), http://www.jishin.go.jp/main/chousa/09_yosokuchizu/g_furoku3.pdf [accessed September 23, 2013]

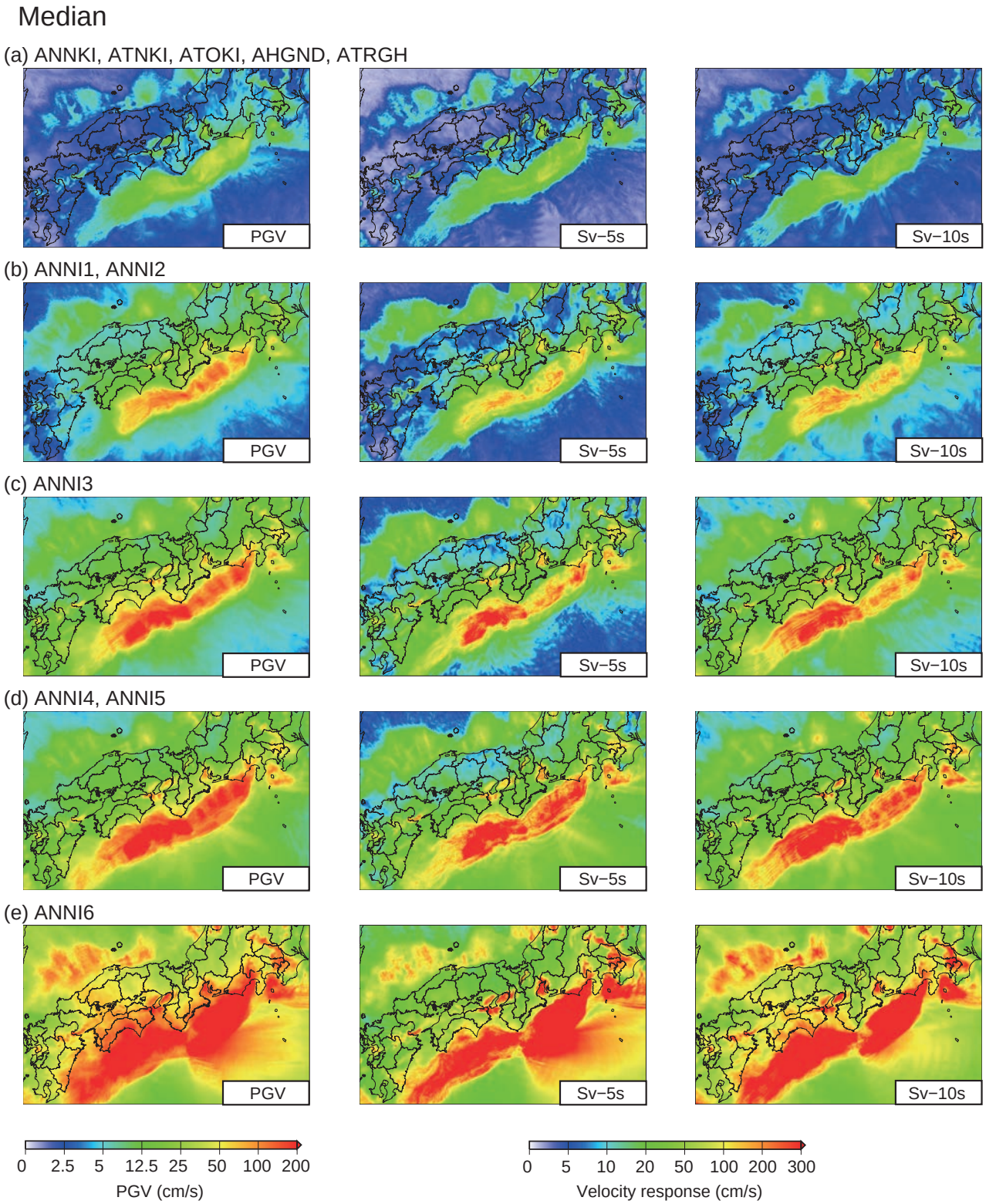

Fig. 9. Peak ground velocity (PGV) and velocity response (S_v) maps showing the median value calculated for five groups. Color scales for PGV and S_v are shown in the bottom.

[8] Earthquake Research Committee, "On the long-term evaluation of earthquakes in the Nankai Trough," 2001 (in Japanese), http://www .jishin.go.jp/main/chousa/01sep_nankai/index.htm [accessed September 23, 2013]

[9] T. Furumura, K. Imai, and T. Maeda, "A revised source model for the 1707 Hoei earthquake and simulation of tsunami inundation of Ryujin Lake, Kyushu, Japan," Journal of Geophysical Research, Vol.116, B02308, doi:10.1029/2010JB007918, 2011.

[10] J. D. Eshelby, "The determination of the elastic field of an ellipsoidal inclusion, and related problems," Proceedings of the Royal Society, Vol.A241, pp. 376-396, 1957.

[11] H. Kanamori and D. Anderson, "Theoretical basis of some empirical relations in seismology," Bulletin of the Seismological Society of America, Vol.65, pp. 1073-1095, 1975.

[12] B. P. Allmann and P. M. Shearer, "Global variations of stress drop for moderate to large earthquakes," Journal of Geophysical Re-

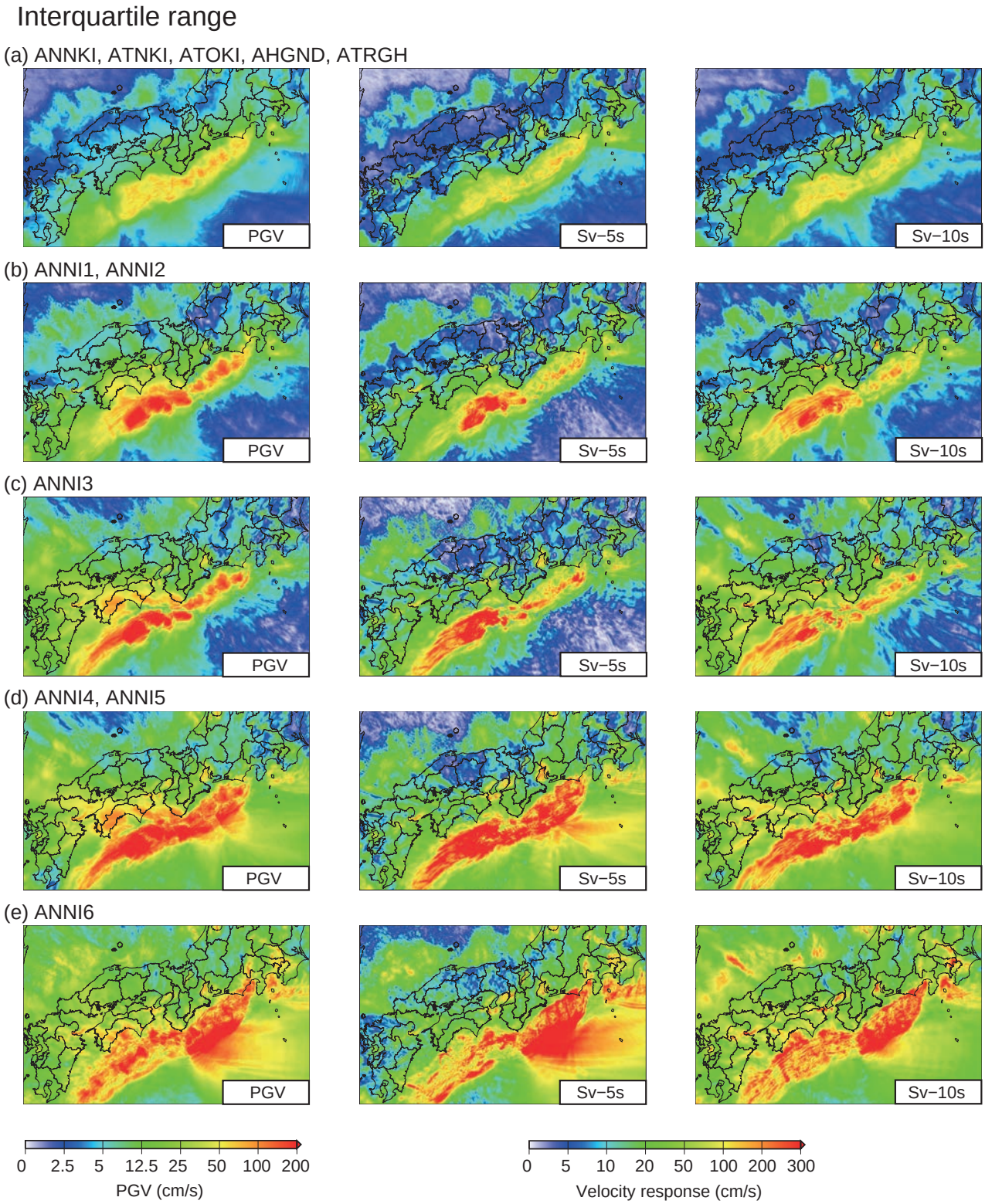

Fig. 10. Peak ground velocity (PGV) and velocity response (S_v) maps showing the interquartile range calculated for five groups. Color scales for PGV and S_v are shown in the bottom.

search, Vol.114, B01310, doi: 10.1029/2008JB005821, 2009.

[13] S. Murotani, H. Miyake, and K. Koketsu, "Scaling of characterized slip models for plate-boundary earthquakes," Earth, Planets and Space, Vol.60, pp. 987-991, 2008.

[14] A. Herrero and P. Bernard, "A kinematic self-similar rupture process for earthquakes," Bulletin of the Seismological Society of America, Vol.84, pp. 1216-1228, 1994.

[15] H. Nakamura and T. Miyatake, "An approximate expression of slip velocity time functions for simulation of near-field strong ground motion," Zisin, Vol.53, pp. 1-9, 2000 (in Japanese with English abstract).

[16] T. Lay, H. Kanamori, C. J. Ammon, K. D. Koper, A. R. Hutko, L. Ye, H. Yue, and T. M. Rushing, "Depth-varying rupture properties of subduction zone megathrust faults," Journal of Geophysical Research, Vol.117, B04311, doi:10.1029/2011JB009133, 2012.

[17] R. J. Geller, "Scaling relations for earthquake source parameters

and magnitudes," Bulletin of the Seismological Society of America, Vol.66, pp. 1501-1523, 1976.
[18] S. Aoi and H. Fujiwara, "3-D finite difference method using discontinuous grids," Bulletin of the Seismological Society of America, Vol.89, pp. 918-930, 1999.
[19] S. Aoi, T. Hayakawa, and H. Fujiwara, "Ground motion simulator: GMS," Butsuri Tansa. Vol.57, pp. 651-666, 2004 (in Japanese with English abstract).
[20] K. Koketsu, H. Miyake, H. Fujiwara, and T. Hashimoto, "Progress towards a Japan integrated velocity structure model and long-period ground motion hazard map," Proceedings of the 14th World Conference on Earthquake Engineering, S10-038, 2008.
[21] R. W. Graves, "Simulating seismic wave propagation in 3D elastic media using staggered grid finite differences," Bulletin of the Seismological Society of America, Vol.86, pp. 1091-1106, 1996.
[22] P. Wessel and W. H. F. Smith, "New version of the Generic Mapping Tools released," Eos Transactions, American Geophysical Union, Vol.76, p. 329, 1995.

Name:
Takahiro Maeda

Affiliation:
Research Fellow, National Research Institute for Earth Science and Disaster Prevention

Address:
3-1 Tennodai, Tsukuba, Ibaraki 305-0006, Japan

Brief Career:
2004 Postdoctoral Fellow, Hokkaido University
2009 Postdoctoral Fellow, University of California, Santa Barbara
2010 Research Fellow, National Research Institute for Earth Science and Disaster Prevention

Selected Publications:
• T. Maeda and T. Sasatani, "Strong ground motions from an Mj 6.1 inland crustal earthquake in Hokkaido, Japan: the 2004 Rumoi earthquake," Earth, Planets and Space, Vol.61, pp. 689-701, 2009.

Academic Societies & Scientific Organizations:
• Seismological Society of Japan (SSJ)
• Japan Association of Earthquake Engineering (JAEE)
• Architectural Institute of Japan (AIJ)
• American Geophysical Union (AGU)

Name:
Nobuyuki Morikawa

Affiliation:
Senior Researcher, National Research Institute for Earth Science and Disaster Prevention

Address:
Tennodai 3-1, Tsukuba-shi, Ibaraki 305-0006, Japan

Brief Career:
2001- National Research Institute for Earth Science and Disaster Prevention

Academic Societies & Scientific Organizations:
• Seismological Society of Japan (SSJ)
• Japan Association for Earthquake Engineering (JAEE)

Name:
Asako Iwaki

Affiliation:
Research Fellow, National Research Institute for Earth Science and Disaster Prevention

Address:
3-1 Tennodai, Tsukuba, Ibaraki 305-0006, Japan

Brief Career:
2011 Dr. of Science, Kyoto University
2011 Research Fellow, National Research Institute for Earth Science and Disaster Prevention

Selected Publications:
• A. Iwaki and T. Iwata, "Estimation of three-dimensional boundary shape of the Osaka sedimentary basin by waveform inversion," Geophysical Journal International, Vol.186, Issue 3, pp. 1255-1278, 2011.
• A. Iwaki and T. Iwata, "Simulation of long-period ground motion in the Osaka sedimentary basin: performance estimation and the basin structure effects," Geophysical Journal International, Vol.181, Issue 2, pp. 1062-1076, 2010.

Academic Societies & Scientific Organizations:
• Seismological Society of Japan (SSJ)
• Architectural Institute of Japan (AIJ)
• Japan Association for Earthquake Engineering (JAEE)
• American Geophysical Union (AGU)

Name:
Shin Aoi

Affiliation:
Director, Earthquake and Volcano Data Center, Earthquake and Volcano Research Unit, National Research Institute for Earth Science and Disaster Prevention (NIED)

Address:
3-1 Tennodai, Tsukuba, Ibaraki 305-0006, Japan

Brief Career:
1996- Researcher, NIED
2002- Senior Researcher, NIED
2013- Principal Senior Researcher, NIED
(2010- Director, Earthquake and Volcano Data Center, Earthquake and Volcano Research Unit, NIED)

Selected Publications:
• S. Aoi, T. Kunugi, and H. Fujiwara, "Trampoline effect in extreme ground motion," Science, Vol.322, pp. 727-730, 2008.
• S. Aoi, B. Enescu, W. Suzuki, Y. Asano, K. Obara, T. Kunugi, and K. Shiomi, "Stress transfer in the Tokai subduction zone from the 2009 Suruga Bay earthquake in Japan," Nature Geoscience, Vol.3, pp. 496-500, 2010.

Academic Societies & Scientific Organizations:
• Seismological Society of Japan (SSJ)
• American Geophysical Union (AGU)

Name:
Hiroyuki Fujiwara

Affiliation:
Director, Department of Integrated Research on Disaster Prevention, National Research Institute for Earth Science and Disaster Prevention

Address:
3-1 Tennodai, Tsukuba, Ibaraki 305-0006, Japan

Brief Career:
1989- Researcher, NIED
2001- Head of Strong Motion Observation Network Laboratory, NIED
2006- Project Director, Disaster Prevention System Research Center, NIED
2011- Director, Social System Research Department, NIED

Academic Societies & Scientific Organizations:
- Seismological Society of Japan (SSJ)
- Japan Association for Earthquake Engineering (JAEE)